Diurnal land surface energy balance partitioning estimated from the thermodynamic limit of a cold heat engine

Axel Kleidon[1] and Maik Renner[1]

[1]Biospheric Theory and Modelling Group, Max-Planck-Institut für Biogeochemie, Jena, Germany

Correspondence to: Axel Kleidon (akleidon@bgc-jena.mpg.de)

Abstract. Turbulent fluxes strongly shape the conditions at the land surface, yet they are typically formulated in terms of semi-empirical parameterizations that make it difficult to derive theoretical estimates of how global change impacts land surface functioning. Here, we describe these turbulent fluxes as the result of a thermodynamic process that generates work to sustain convective motion and thus maintains the turbulent exchange between the land surface and the atmosphere. We first derive a limit from the second law of thermodynamics that is equivalent to the Carnot limit, but which explicitly accounts for diurnal heat storage changes in the lower atmosphere. We then use this limit of a cold heat engine together with the surface energy balance to infer the maximum power that can be derived from the turbulent fluxes for a given solar radiative forcing. The surface energy balance partitioning estimated from this thermodynamic limit requires no empirical parameters and compares very well with the observed partitioning of absorbed solar radiation into radiative and turbulent heat fluxes across a range of climates, with correlation coefficients $r^2 \geq 95$ % and slopes near one. These results suggest that turbulent heat fluxes on land operate near their thermodynamic limit on how much convection can be generated from the local radiative forcing. It implies that this type of approach can be used to derive first-order estimates of global change that are solely based on physical principles.

1 Introduction

The turbulent fluxes of sensible and latent heat play a critical role for the land surface energy balance during the day as these fluxes represent the principal means by which the surface cools and exchanges moisture, carbon dioxide and other compounds with the atmosphere. Due to their inherent complex nature, these fluxes are typically being described by semi-empirical expressions (e.g., Businger et al., 1971; Louis, 1979; Beljaars and Holtslag, 1991). Yet, representations of this exchange in land surface and climate models are still associated with a high degree of uncertainty. This uncertainty results, for instance, in biases in evapotranspiration and surface temperatures across different models (Mueller and Seneviratne, 2014), in empirical relationships of land surface exchange outperforming land surface models (Best et al., 2015), and in by biases in boundary layer heights (Davy and Esau, 2016). The semi-empirical and highly coupled nature of land surface-atmosphere exchange seems to make it almost impossible to derive simple, physically-based estimates of the magnitude of turbulent exchange and how it changes with land cover change or global warming.

An alternative approach to describe surface-atmosphere exchange can be based on thermodynamics (Kleidon et al., 2014; Dhara et al., 2016), an aspect that is rarely considered in the description of surface-atmosphere exchange. In this approach,

turbulent exchange is formulated as a thermodynamic process by which turbulent heat fluxes drive a convective heat engine within the atmosphere that yields the work to maintain convection and thus the turbulent exchange near the surface. This approach specifically invokes the second law of thermodynamics as an additional constraint on atmospheric dynamics (similar to previous approaches, such as Paltridge, 1978; Ozawa and Ohmura, 1997; Lorenz et al., 2001; Ozawa et al., 2003). The second

5 law sets a limit to how much work can be derived from the local radiative forcing of the system. The dynamics associated with convection are then essentially captured by the implicit assumption that convection works as hard as it can, so that the use of the thermodynamic limit approximates the emergent convective dynamics. Previous applications of this thermodynamic approach have shown that it can successfully describe the broad climatological variation of surface energy balance partitioning on land and ocean (Kleidon et al., 2014; Dhara et al., 2016), the strength and sensitivity of the hydrologic cycle and surface temperatures

10 to global change (Kleidon and Renner, 2013a, b; Kleidon et al., 2015; Kleidon and Renner, 2017), and the dynamics of the Earth system in general (Kleidon, 2016).

Here we extend this approach to the diurnal variation of the surface energy balance on land and compare its estimated partitioning to observations across different climates. As in the previous applications of thermodynamics to land-atmosphere exchange, the starting point is to view turbulent fluxes as the result of a heat engine that is driven by these heat fluxes (Fig. 1).

15 The limit to how much work this heat engine can maximally perform is set by the first and second law of thermodynamics, from which the well-known Carnot limit of a heat engine can be derived (e.g., Kleidon, 2016).

When applied to the setting of the diurnal cycle of the land-atmosphere system, two key aspects need to be considered as these shape the thermodynamic limit (as illustrated in Fig. 1 by the two boxes on the right). First, the strong diurnal variation of solar radiation causes strong changes in heat storage within the system that result in a much less varying emission of terrestrial

20 radiation to space. In the absence of such heat storage changes, nighttime temperatures would be much colder than those found on Earth. In the ideal case that is being considered here, the strong variation of solar radiation is completely leveled out to yield a uniform emission of radiation to space, as indicated by the blue line in the graph at the top of Fig. 1 labeled $R_{l,out}$. While these heat storage changes predominantly take place below the surface for open water surfaces such as the ocean and lake systems (reflected in nearly uniform turbulent fluxes during night and day, see, e.g., measurements by Liu et al., 2009), the

25 land-atmosphere system accommodates these changes mostly in the lower atmosphere (Kleidon and Renner, 2017) because heat diffusion into the soil is slow (Oke, 1987). The relevance of this different way to accommodate heat storage changes over land is that it takes place within the heat engine that we consider. The heat storage change is associated with a heating of the engine during the day, which represents an additional term of the entropy balance of the engine. What we show here is that the resulting thermodynamic limit is somewhat different to the common Carnot limit and we refer to this limit as the Carnot limit

30 of a cold heat engine.

The magnitude of the diurnal variation in heat storage is well constrained when assuming that the radiative heating by solar radiation and the emission to space are roughly balanced over the course of day and night. The temporal change of heat storage during the day can then be inferred from the imbalance of radiative fluxes at the top of the atmosphere (indicated in the upper panel at the right of Fig. 1, and as described by Kleidon and Renner, 2017).
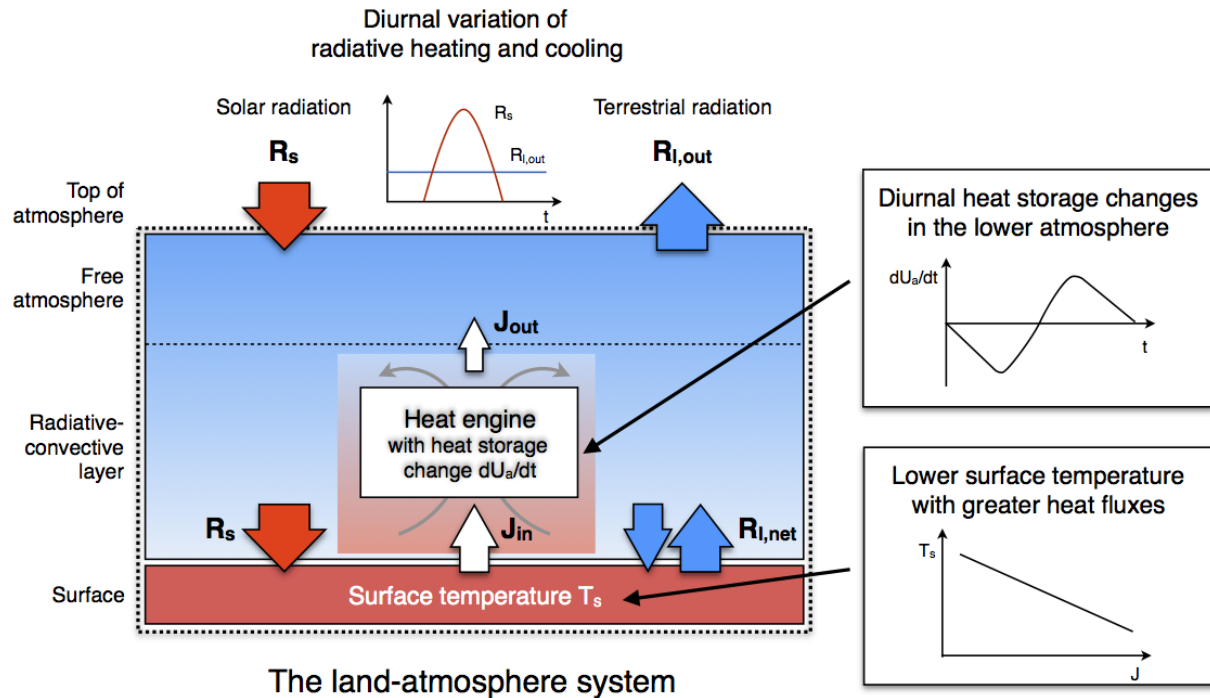
Figure 1. Schematic diagram of the surface-atmosphere system where turbulent heat fluxes from the surface, J_{in}, act as the driver of an atmospheric heat engine that generates convective motion and which sustains the heat fluxes. The heat source of the engine is the absorption of solar radiation at the surface, R_s, reduced by the net exchange of terrestrial radiation, $R_{l,net}$, which depends on surface temperature. The two critical effects that set the limit to how much work the engine can perform are illustrated on the right: Diurnal changes in heat storage in the lower atmosphere due to the diurnal variation of solar radiation and the reduction of surface temperature, T_s, due to greater turbulent heat fluxes both lower the work output of the engine.

The second aspect that shapes the thermodynamic limit is the reduction of surface temperature in the presence of greater turbulent fluxes at the surface (lower panel at the right of Fig. 1). This reduction of surface temperature reduces the temperature difference that is utilized by the heat engine to derive power, thus setting a limit of maximum power of the heat engine (as in, e.g., Kleidon and Renner, 2013a; Kleidon et al., 2014; Dhara et al., 2016) and also in closely related studies using the proposed principle of Maximum Entropy Production (Ozawa and Ohmura, 1997). We then combine the thermodynamic limit of a cold heat engine with the energy balances of the surface and of the whole surface-atmosphere system, and maximize the power output of the heat engine to get a fully constrained description of the system that can, in first approximation, be solved analytically. It yields a description of the turbulent exchange between the land surface and the atmosphere that is fully constrained by thermodynamics and free of empirical turbulence parameterizations.

In the following, we first derive the thermodynamic limit of a cold heat engine, combine it with the energy balances of the system and maximize the power output to estimate surface energy balance partitioning based on the solar forcing of the system. The estimated partitioning is then tested with observations across field sites of contrasting climatological conditions.

We then discuss how our thermodynamic approach compares to the common approaches in boundary layer meteorology and the potential implications of our approach.

2 Thermodynamic formulation of the land surface energy balance

We consider the land surface-atmosphere system as a thermodynamic system in a steady state when averaged over the diurnal cycle. Surface heating by absorption of solar radiation, R_s, causes the surface to warm, while the atmosphere is cooled by the emission of radiation to space, $R_{l,out}$ (Fig. 1). The surface and atmosphere are linked by the net exchange of terrestrial radiation, $R_{l,net}$, and turbulent heat fluxes, J_{in}, that result from convective motion. We consider this system as a locally forced system with no advection. Convective motion within the boundary layer is seen as the consequence of a heat engine that generates motion out of the turbulent heat fluxes, where, for simplicity, we do not distinguish between the effects of the sensible and latent heat flux and the associated forms of dry and moist convection. The steady state condition is used for the radiative forcing of the whole system by requiring that the mean radiative fluxes taken over the whole day are balanced such that $R_s = R_{l,out}$. Furthermore, we assume that generation of turbulent kinetic energy, or power, G (or work per time), and its frictional dissipation, D, are in balance, so that $G = D$. In the following, we derive the limit to how much power can be derived from the forcing of the system directly from the first and second law of thermodynamics in a general way, so that we do not need to make the assumption that the atmosphere operates in a Carnot-like cycle. All variables used in the following are summarized and described in Table 1.

2.1 Carnot limit with heat storage changes

We first derive a thermodynamic limit akin to the Carnot limit from the energy and entropy balances of the heat engine which specifically includes the change in heat storage within the engine. The first law of thermodynamics applied to this setup is given by

$$\frac{dU_a}{dt} = J_{in} + D - J_{out} - G \tag{1}$$

where dU_a/dt is the change in heat storage within the lower atmosphere, J_{in} represents the addition of heat by the turbulent heat fluxes from the surface, J_{out} is the rate by which the heat engine is being cooled, which is accomplished by radiative cooling. Note that this formulation differs from the derivation of the Carnot limit by accounting for changes in internal energy on the left-hand side and for dissipative heating, D, on the right-hand side as frictional dissipation takes place within the system. As we consider a steady state with $G = D$, note that the contributions of these terms in eqn. 1 cancel out so that the equation reduces to $dU_a/dt = J_{in} - J_{out}$.

The associated entropy budget of the heat engine is given by a change in entropy associated with the change in heat storage, dU_a/dt, at an effective engine temperature T_e, the entropy input by J_{in} at a temperature T_s, the entropy export by J_{out} at a temperature T_a, and frictional dissipation that is assumed to occur at temperature T_e, and possibly some irreversible entropy

production σ_{irr} within the engine:

$$\frac{1}{T_e}\frac{dU_a}{dt} = \frac{J_{in}}{T_s} + \frac{D}{T_e} - \frac{J_{out}}{T_a} + \sigma_{irr} \tag{2}$$

For the atmospheric temperature, T_a, we use the radiative temperature associated with $R_{l,out}$ (i.e., we use the Stefan-Boltzmann law, $R_{l,out} = \sigma T_a^4$ to infer T_a, with $\sigma = 5.67 \cdot 10^{-8}$ W m^{-2} K-4 being the Stefan-Boltzmann constant). This

5   is the most optimistic temperature for the entropy export from the heat engine as it is the coldest temperature possible to emit radiation at a rate $R_{l,out}$ to space and thus represents the highest entropy export from the heat engine (note that blackbody radiation represents the radiative flux with maximum entropy). Note also that this temperature is not bound to a particular height within the atmosphere, but is rather inferred from the energy balance constraint. The effective engine temperature, T_e, essentially represents the potential temperature of the lower atmosphere as the temperature variation within the lower atmosphere is

10   shaped by convection and is thus approximately adiabatic.

The thermodynamic limit to how much power, G, can maximally be derived by the engine is obtained from the entropy budget using the ideal case in which $\sigma_{irr} = 0$ (the second law of thermodynamics requires $\sigma_{irr} \geq 0$). Using Eq. (1) to replace J_{out} in Eq. (2), we obtain:

$$G = J_{in} \cdot \frac{T_e}{T_a} \cdot \frac{T_s - T_a}{T_s} - \frac{dU_a}{dt} \cdot \frac{T_e - T_a}{T_a} \tag{3}$$

15   In this expression, the temperature of the heat engine, T_e, plays an important role. In the limiting case of $T_e \approx T_a$, this expression reduces to the common Carnot limit as the effect of the change in heat content is indistinguishable from the waste heat flux, J_{out}, of the heat engine. As the engine temperature essentially represents the potential temperature of the lower atmosphere, it is much closer to the surface temperature, so that the approximation $T_e \approx T_s$ is better justified. With this approximation, the thermodynamic limit of power then reduces to:

20   $$G \approx \left(J_{in} - \frac{dU_a}{dt} \right) \cdot \frac{T_s - T_a}{T_a} \tag{4}$$

In the absence of heat storage changes, the term dU_a/dt vanishes and yields, again, the common Carnot limit, except that T_a appears in the denominator of the Carnot efficiency rather than T_s, an aspect that has previously been derived in the context of a "dissipative" heat engine (Renno and Ingersoll, 1996; Bister and Emanuel, 1998). Note that in the presence of positive heat storage changes, as is the case during the day, the maximum power that can be derived from the heat flux J_{in} is reduced. That

25   is, the increase in heat storage within the engine ($dU_a/dt > 0$) results in a lower efficiency in converting heat into power (with the efficiency given by the ratio G/J_{in}), as would be expected of a cold heat engine.

2.2 Energy balance constraints

We next use the energy balance constraints of the surface and the whole system to express dU_a/dt and $T_s - T_a$ in terms of the absorption of solar radiation at the surface, R_s, and the turbulent heat flux J_{in}. This will allow us to replace these two terms in

30   Eq. (4), so that the power G only depends on R_s and J_{in}.

The surface energy balance constrains the relationship between the heat flux J_{in} and the temperature difference that drives the heat engine, $T_s - T_a$. We express this balance by

$$R_s - k(T_s - T_a) - J_{in} - \frac{dU_s}{dt} = 0 \tag{5}$$

where we linearize the net longwave radiative exchange, $R_{l,net} = k(T_s - T_a)$, between the surface and the atmosphere and where dU_s/dt describes heat storage changes below the surface, which is represented by the ground heat flux. This formulation of the surface energy balance can be used to express the temperature difference, $T_s - T_a$, as a function of R_s, J_{in}, and heat storage changes at the surface, dU_s/dt.

The energy balance of the whole system, neglecting heat advection terms, yields a constraint of the form

$$\frac{dU_{tot}}{dt} = \frac{dU_a}{dt} + \frac{dU_s}{dt} = R_s - R_{l,out} = R_s - R_{s,avg} \tag{6}$$

where $dU_{tot}dt$ is the total change in heat storage within the surface-atmosphere system. We assume this balance to be in a steady state when averaged over day and night, so that on average, $R_{l,out} = R_{s,avg}$, where $R_{s,avg}$ is the temporal mean of R_s taken over the whole day. The energy balance of the whole system provides an expression for dU_a/dt as a function of the instantaneous value of absorbed solar radiation, R_s, the mean absorption of solar radiation, $R_{s,avg}$, and the ground heat flux, dU_s/dt.

2.3 Maximization of convective power

The surface energy balance (Eq. 5) can now be used to express the temperature difference that drives the heat engine, $T_s - T_a$, in the thermodynamic limit given by Eq. (4), while the energy balance of the whole system (Eq. 6) can be used to constrain the terms describing the changes in heat storage, dU_a/dt. As the power G is an increasing function of J_{in}, but the temperature difference declines with greater values of J_{in}, the power has a maximum, which is referred to as the maximum power limit. This limit can be derived analytically by $\partial G/\partial J_{in} = 0$ and is associated with an optimum heat flux of the form

$$J_{opt} \approx \frac{1}{2}\left(R_s - \frac{dU_s}{dt} + \frac{dU_a}{dt}\right) \tag{7}$$

This expression is similar to previous work where the optimum heat flux is given by $R_s/2$ in the absence of heat storage changes (Kleidon and Renner, 2013a, b). It is, however, modulated by heat storage changes, and it matters whether these changes take place below the surface or in the lower atmosphere as the two forms of heat storage changes enter Eq. (7) with a different sign. Note that in the limiting case $dU_s/dt \approx dU_{tot}/dt$ (like an open water surface), the optimum heat flux reduces to $J_{opt} \approx R_{s,avg}/2$, while in the contrasting case of $dU_a/dt \approx dU_{tot}/dt$, the optimum heat flux is $J_{opt} \approx R_s - R_{s,avg}/2$. Hence, information of absorbed solar radiation (and the ground heat flux to account for dU_s/dt) are sufficient to estimate surface energy balance partitioning from the thermodynamic limit of maximum power.

2.4 Evaluation of the approach

To evaluate our estimate, it requires observations of absorbed solar radiation during the day, R_s, and the ground heat flux, dU_s/dt. From the diurnal course of R_s, the mean value of $R_{s,avg}$ can be calculated, which in turn yields an estimate for

dU_{tot}/dt. Taken together with the ground heat flux, this yields the value of dU_a/dt, so that all terms in Eq. 7 can be specified. The resulting estimate of J_{opt} can then be compared to observations of the turbulent heat fluxes, or to the available energy, i.e. net radiation reduced by the ground heat flux.

3 Data sources

5 We use two types of data sources to test our approach. To test how reasonable the estimates are for the diurnal heat storage changes in the lower atmosphere, we first use six-hourly radiosonde data from the DWD meteorological observatory Lindenberg in Brandenburg, Germany (data available at http://weather.uwyo.edu/upperair/sounding.html). We use data from this site because this observatory provides a long and consistent record of four vertical profiles a day as well as surface energy balance components, while typically only two vertical profiles a day are taken. We use observations from June for the years 2006 to
10 2009 and calculate the moist static energy at each six-hour interval and then take the difference over the time interval to obtain estimates for changes in atmospheric heat storage. These differences are then compared to the change in atmospheric heat storage expected from solar radiation, as described by Eq. (6).

We then use observations of absorbed solar radiation (R_s) and the ground heat flux (dU_s/dt) at six field sites in highly contrasting climatological settings (listed in Table 2) to calculate the turbulent heat fluxes from maximum power (Eq. 7). The
15 six sites include two observation sites at Lindenberg, Brandenburg, Germany (a grassland site and a forested site Beyrich et al., 2006), three AmeriFlux sites (Rocha and Shaver (a tundra site at Anaktuvuk River, Alaska 2011); a grassland site at Southern Great Plains, Oklahoma Fischer et al. (2007); Raz-Yaseef et al. (2015); and a tropical rainforest site at Tapajos National Park, Brazil, Goulden et al. (2004)) and a site in a planted pine forest at Yatir forest in Israel (Rotenberg and Yakir, 2010, 2011). For each site, we use one month of observations for a summer period in which solar radiative heating of the surface is highest and
20 the effects of heat advection are minor, estimate turbulent fluxes associated with maximum power (using Eq. 7), and compare these to the observed fluxes.

4 Results

We first evaluate the extent to which diurnal variations in solar radiation are buffered by heat storage changes in the lower atmosphere. To do so, we use the diagnosed variations of moist static energy from the radiosoundings in Lindenberg, Germany
25 and compare these to the mean variation in absorbed solar radiation at the surface as well as variations in the ground heat flux at the site in Fig. 2. The comparison shows that the heat storage variations in the lower atmosphere are substantially greater than the ground heat flux so that the diurnal variations in solar radiation are mostly buffered by the lower atmosphere. Although there is considerable variation, mostly due to pressure changes and advective effects, these variations follow the temporal course of what is expected from the variation in absorbed solar radiation (as described by Eq. 6). This confirms our conjecture
30 that the diurnal variations in solar radiation on land are buffered primarily by heat storage changes in the lower atmosphere. This buffering of the diurnal variations over the land surface is rather different to how an open water surface buffers these

A. Heat storage mechanisms
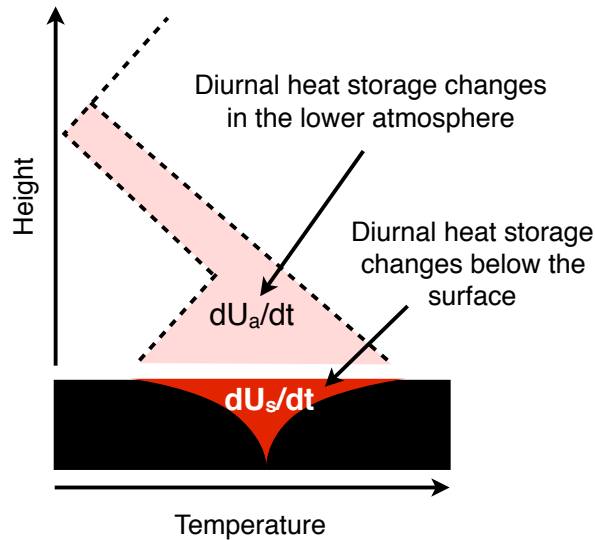
B. Observations in Lindenberg
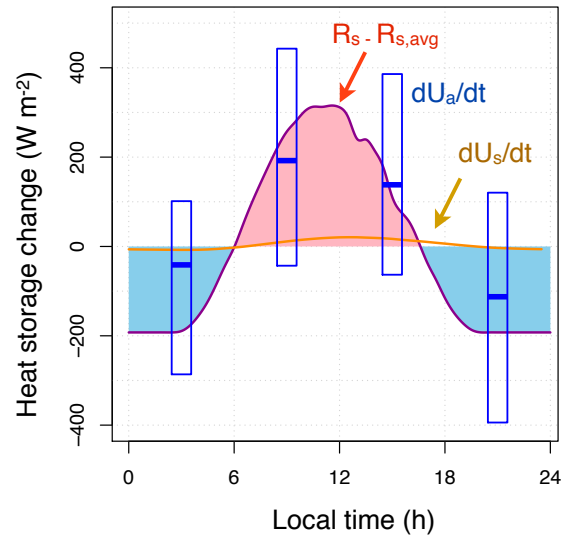
Figure 2. Diurnal changes in heat storage are reflected in variations of soil temperature near the surface and in variations of air temperature and humidity in the lower atmosphere. Panel (a.) shows a schematic diagram of these heat storage changes, and (b.) shows observations from Lindenberg, Germany. Panel (b.) shows the mean diurnal variation of absorbed solar radiation, R_s, averaged for the month of June over the years 2006-2009 (red line, $n = 480$), the diurnal variation in heat storage in the lower atmosphere derived from six-hourly radiosoundings, dU_a/dt, (blue bars) and the ground heat flux, dU_s/dt (orange line). Absorbed solar radiation has been shifted such that the mean of R_s taken over the day is zero, consistent with our approximation of a steady state when averaged over the whole day.

variations (as also shown by observations (Liu et al., 2009), and an aspect used previously to explain the difference in climate sensitivity of land and ocean surfaces (Kleidon and Renner, 2017)).

The comparison of the estimated energy flux partitioning from maximum power to observations at the six sites is shown in Fig. 3. The correlations are summarized in Table 2 in terms of the correlation coefficient as well as the slope and intercept.

5   During nighttime, there is a mismatch between our approach and observations, which is represented by the intercept shown in Table 2. This mismatch may be explained by the prevalent stable nighttime conditions in which the atmosphere does not act as a heat engine, an aspect that we did not consider in our approach. During daytime, we find very high correlations of above 95% between the estimated turbulent fluxes from the maximum power limit with observed net radiation (reduced by the ground heat flux), with a very good match of the estimated slopes in the correlation within 15% of the observed. This high level of

10   agreement is found across the range of climatological settings shown in Fig. 3.

Also note that the maximum power limit without an explicit consideration of heat storage changes (i.e., with $dU_s/dt = 0$ and $dU_a/dt = 0$ in Eq. (7), as in Kleidon et al. (2014)) and as indicated by light blue points, estimates turbulent fluxes that also result in a high correlation, but with a magnitude that is too low compared to observations. This high level of agreement of the
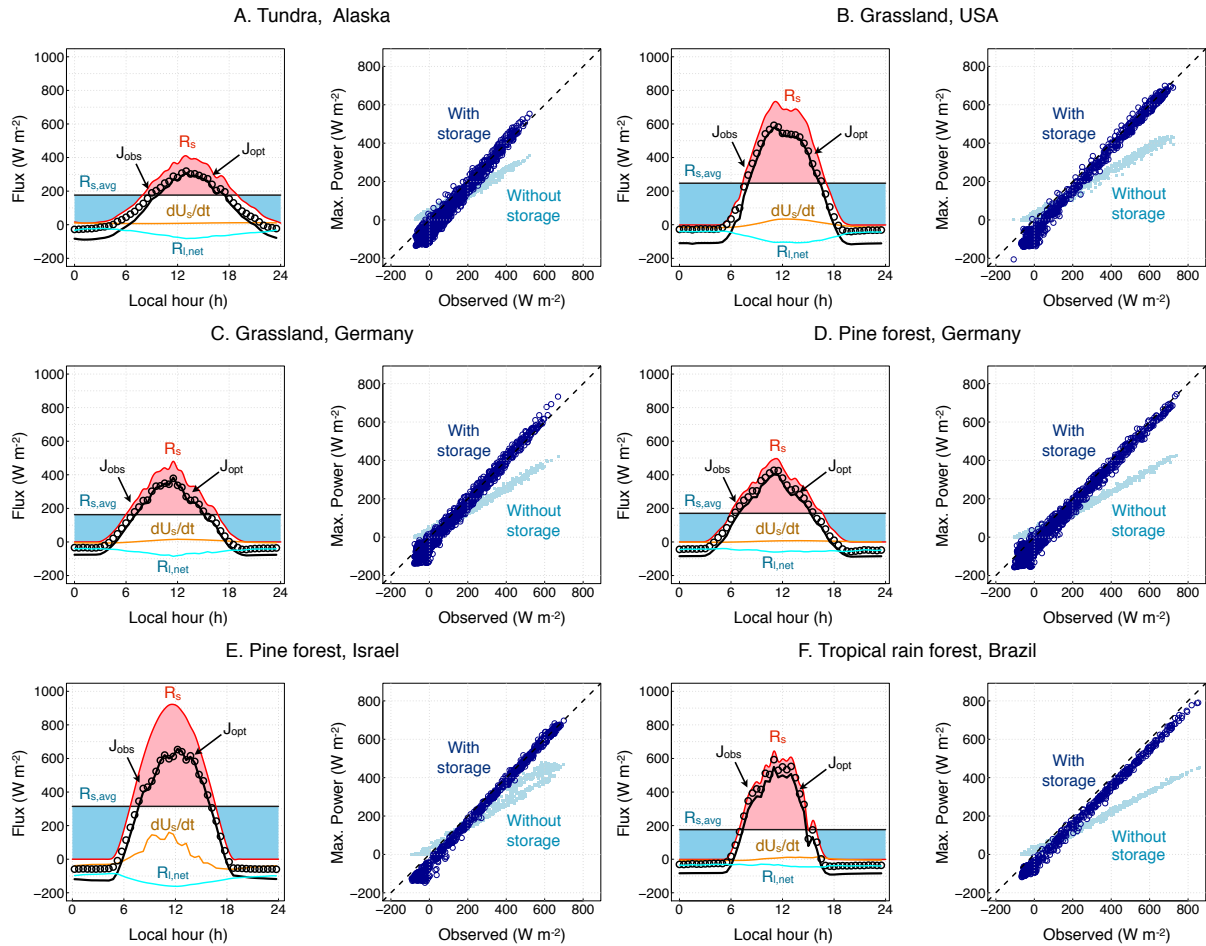
Figure 3. Mean diurnal cycle of absorption of solar radiation at the surface (R_s, red line, observed), ground heat flux (dU_s/dt, orange line, observed), and turbulent heat fluxes estimated by maximum power (J_{opt}, black line, estimated) and observations (J_{obs}, black circles, observed) for a selected month for six field observations in (A) a tundra ecosystem in Alaska, (B) a cropland in the Midwestern US, (C, D) a grassland and pine forest in a temperate environment in Germany, (E) a planted pine forest in an arid environment in Israel, and (F) a tropical rainforest in the humid Amazon basin in Brazil. The comparison of the turbulent heat fluxes estimated from maximum power to energy balance measurements is shown for 30 minute observations in the right panel for each site for two cases of thermodynamic limits that differ by their consideration of heat storage changes in the thermodynamic limit (dark blue: with storage, as in Eq. (4); light blue: without storage, i.e. $dU_s/dt = 0$ and $dU_a/dt = 0$ so that $J_{opt} = R_s/2$). More information on the sites as well as the correlation statistics are provided in Table 2.

maximum power limit with diurnal heat storage changes suggests that it is an adequate description of surface energy balance partitioning and land surface-atmosphere exchange at the diurnal time scale, so that turbulent fluxes appear to operate near their

thermodynamic limit. It further shows that it is critical to account for diurnal variations in heat storage in the thermodynamic limit to adequately represent the magnitude of the observed turbulent fluxes.

5 Discussion

Our approach represents, of course, only a first-order description of the full dynamics of surface-atmosphere exchange. Notable
5 effects not considered in our approach that could alter the results and potentially modulate the outcome of the maximum power limit include a more detailed representation of radiative transfer, a distinction between the sensible and latent heat fluxes which result in different forms of storage changes in the atmosphere, entrainment effects at the top of the boundary layer, advection and coupling to large-scale atmospheric processes, and a better representation of nighttime processes, particularly regarding the formation of stable conditions at night that prevent convection to occur. These aspects can be explored further in future
10 extensions. Yet, even at this highly simplified level, the agreement of the estimated flux partitioning with observations is rather remarkable, indicating that the dominant forcing and the dominant constraints are captured by our approach.

Our results emphasize the importance to consider the constraint imposed by the second law of thermodynamics on land-atmosphere exchange. While the complex, turbulent nature of this exchange make it seem almost impossible to describe its outcome in simple terms, the generation of turbulent kinetic energy that drives the diurnal development of the convective
15 boundary layer is nevertheless constrained by thermodynamics. The very good agreement of our results with observations suggests that this constraint imposed by thermodynamics is relevant to this generation, and land-atmosphere exchange appears to operate near this thermodynamic limit. This is consistent with previous research that applied thermodynamics and/or heat engine frameworks to atmospheric motion, for instance approaches using the proposed principle of Maximum Entropy Production (Paltridge, 1978; Ozawa and Ohmura, 1997; Lorenz et al., 2001; Ozawa et al., 2003) or applications to hurricanes and
20 atmospheric convection (Emanuel, 1999; Pauluis and Held, 2002a, b). Note that our maximization of power almost identical to the maximization of material entropy production, as we assume a steady state in which power equals dissipation ($G = D$), and entropy production by turbulence is then given by D/T, where T is the temperature at which dissipation occurred (with $T \approx T_s$). Yet, our approach differs in that it specifically considered the effect of heat storage changes in altering the thermodynamic limit and feedbacks with the surface energy balance that altered the driving temperature difference of the heat engine.
25 The heat storage changes in the lower atmosphere result in an additional term in the Carnot limit, and this can explain why the land-atmosphere system functions quite differently with its pronounced diurnal variations in turbulent fluxes in contrast to the temporally much more uniform turbulent fluxes over open water surfaces (e.g., Liu et al., 2009; Kleidon, 2016; Kleidon and Renner, 2017). Thermodynamics combined with these two additional factors then provide sufficient constraints to the magnitude of turbulent heat fluxes. It would seem that this could provide valuable information to better parameterize turbulent fluxes
30 within the Monin-Obukhov similarity theory for unstable conditions, specifically regarding the stability functions that are used in this approach (e.g., as in Louis, 1979).

This insight that surface energy balance partitioning is predominantly determined by the local partitioning of the absorbed solar radiation is rather different than the way this exchange is commonly represented in climate models. In these models,

surface exchange is parameterized using the aerodynamic bulk approach, in which the aerodynamic drag of the surface and horizontal wind speeds play a dominant role that is modulated by stability functions. Our approach differs in that solar radiation plays the dominant role for surface exchange by local generation of buoyancy and power to drive convection, rather than wind speed and aerodynamic roughness as what the bulk method would suggest. A recent intercomparison between a number of

5 commonly used land surface models (Best et al., 2015) shows, however, that land surface models using the bulk method generally underestimate the strong correlation of turbulent fluxes with downward solar radiation found in observations. Our approach can resolve this bias and suggests that the bulk method may underestimate the effect of the local forcing by solar radiation on surface-atmosphere exchange.

We think that our approach provides ample opportunities for future research. First, the approach should further be evaluated

10 in a broader range of climatological conditions and over extended time periods to identify possible shortcomings, for instance with respect to the simple parameterization of longwave radiation or regarding the omission of advective effects. For a broader range of applicability, the approach would need to be extended further to be able to derive an expression for near-surface air temperature, which would be related to the changes in atmospheric heat storage (dU_a/dt), for the aerodynamic conductance, and for boundary layer development, and the turbulent heat fluxes should be separated into the fluxes of sensible and latent

15 heat. The approach may also help to improve the semi-empirical parameterizations of surface exchange, particularly for unstable conditions. This approach can then be used to evaluate aspects of global change, such as land cover change or global warming, analytically, thus providing an alternative approach to these topics that complements complex, numerical modelling approaches. More generally, the success of our approach in reproducing observations very well constitutes another example that processes in complex systems appear to evolve to and operate at their thermodynamic limit (Ozawa et al., 2003; Martyu-

20 shev and Seleznev, 2006; Kleidon et al., 2010; Kleidon, 2016). This, in turn, encourages the application of thermodynamics to a broader range of questions and topics to understand the evolution and emergent dynamics of complex Earth systems.

6 Conclusions

We formulated a Carnot limit which accounts for heat storage changes within the atmospheric heat engine and used this limit to estimate the partitioning of the solar radiative forcing into radiative and turbulent cooling at the diurnal time scale. In

25 contrast to common approaches to describe near-surface turbulent heat transfer into the atmosphere, we explicitly consider the thermodynamic constraint imposed by the second law of thermodynamics by treating turbulent heat fluxes and convection as the result of a heat engine. The maximization of the work output of this convective heat engine then yields estimates of turbulent fluxes that compare very well to observations across a range of climates and do not require empirical parameterizations. This demonstrates that our approach represents an adequate, first-order description of the land surface energy balance that only uses

30 physical concepts and that does not rely on semi-empirical turbulence parameterizations.

We conclude that boundary layer convection over land appears to operate near its thermodynamic limit by which the power of the convective heat engine is maximized. This limit is shaped by the second law of thermodynamics, as in the case of the Carnot limit of a heat engine in classical thermodynamics, but also requires the consideration of two additional factors that

relate the heat engine to its environmental setting. The first factor relates to the strong diurnal variation of solar radiation, which results in diurnal heat storage changes. Over land these changes are buffered primarily in the lower atmosphere and these modulate the Carnot limit, resulting in a reduced efficiency and in what we referred to as a cold heat engine. Second, the limit of maximum power of the atmospheric heat engine is shaped by the trade-off in the driving temperature difference

5 between surface and atmosphere, which decreases with greater turbulent heat fluxes. This tradeoff results in the maximum power limit and represents a strong coupling between surface conditions and the lower atmosphere.

Overall, our study shows that thermodynamics adds a highly relevant constraint to land-surface atmosphere coupling. This thermodynamic approach to the surface energy balance and land-atmosphere interactions should help us to better understand the role of the land surface and terrestrial vegetation in the climate system and how it interacts with global change.

10 *Competing interests.* The authors have no conflict of interests.

Acknowledgements. We thank Henk de Bruin, Andreas Chlond, Pierre Gentine, and Aljosa Slamersak for constructive discussions on land-atmosphere exchange. This research contributes to the "Catchments As Organized Systems (CAOS)" research group (FOR 1598) funded by the German Science Foundation (DFG). We acknowledge the University of Wyoming for making the radio sounding data available at http://weather.uwyo.edu/upperair/sounding.html. Data from Site A was funded by NSF grant 1556772 to the University of Notre Dame. Data

15 from Site B was supported by the Office of Biological and Environmental Research of the US Department of Energy under contract No. DE-AC02-05CH11231 as part of the Atmospheric Radiation Measurement Program (ARM). Data for Site C and D were provided by the Deutscher Wetterdienst (DWD) - Meteorologisches Observatorium Lindenberg / Richard-Assmann Observatorium. It was obtained in the context of the Coordinated Energy and Water Cycle Observation Project (CEOP), which was initiated as an international effort in 1998 by the World Climate Research Programme (WCRP) Global Energy and Water Cycle Experiment (GEWEX) Hydrometeorology Panel (GHP)

20 in support of global climate research interests. Data for Site E was kindly provided by Eyal Rotenberg and Daniel Yakir. Data for Site F was provided by the AmeriFlux data server, http://ameriflux.ornl.gov.

References

Beljaars, A. C. M. and Holtslag, A. A. M.: Flux Parameterization over Land Surfaces for Atmospheric Models, J. Appl. Meteorol., 30, 327–341, 1991.

Best, M. J., Abramowitz, G., Johnson, H. R., Pitman, A. J., Balsamo, G., Boone, A., Cuntz, M., Decharme, B., Dirmeyer, P. A., Dong, J., Ek,
5   M., Guo, Z., Haverd, V., van den Hurk, B. J. J., Nearing, G. S., Pak, B., Peters-Lidard, C., Jr, J. A. S., Stevens, L., and Vuichard, N.: The plumbing of land surface models: benchmarking model performance, J. Hydrometeorol., 16, 1425–1442, 2015.

Beyrich, F., Leps, J. P., Mauder, M., Bange, J., Foken, T., Huneke, S., Lohse, H., Luedi, A., Meijninger, W. M. L., Mironov, D., Weisensee, U., and Zittel, P.: Area-averaged surface fluxes over the Litfass region based on eddy-covariance measurements, Boundary Layer Meteorology, 121, 33–65, 2006.

10 Bister, M. and Emanuel, K. A.: Dissipative heating and hurricane intensity, Meteorol. Atmos. Phys., 65, 233–240, 1998.

Businger, J. A., Wyngaard, J. C., Izumi, Y., and Bradley, E. F.: Flux-Profile Relationships in the Atmospheric Surface Layer, J. Atmos. Sci., 28, 181–189, 1971.

Davy, R. and Esau, I.: Differences in the efficacy of climate forcings explained by variations in atmospheric boundary layer depth, Nat. Commun., 7, 11 690, doi:10.1038/ncomms11690, 2016.

15 Dhara, C., Renner, M., and Kleidon, A.: Broad climatological variation of surface energy balance partitioning across land and ocean predicted from the maximum power limit, Geophys. Res. Lett., 43, 7686–7693, 2016.

Emanuel, K. A.: Thermodynamic control of hurricane intensity, Nature, 401, 665–669, 1999.

Fischer, M. L., Billesbach, D. P., Riley, W. J., Berry, J. A., and Torn, M. S.: Spatiotemporal Variations in Growing Season Exchanges of CO_2, H_2O, and Sensible Heat in Agricultural Fields of the Southern Great Plains, Earth Interactions, 11, 1–21, 2007.

20 Goulden, M. L., Miller, S. D., da Rocha, H. R., Menton, M. C., de Freitas, H. C., Figuera, A. M. S., and de Sousa, C. A. D.: Diel and seasonal patterns of tropical forest CO_2 exchange, Ecol. Appl., 14, S42–S54, 2004.

Kleidon, A.: Thermodynamic foundations of the Earth system, Cambridge University Press, 2016.

Kleidon, A. and Renner, M.: Thermodynamic limits of hydrologic cycling within the Earth system: concepts, estimates and implications, Hydrol. Earth Syst. Sci., 17, 2873–2892, 2013a.

25 Kleidon, A. and Renner, M.: A simple explanation for the sensitivity of the hydrologic cycle to climate change, Earth Syst. Dynam., 4, 455–465, doi:10.5194/esd-4-455-2013, 2013b.

Kleidon, A. and Renner, M.: An explanation for the different climate sensitivities of land and ocean surfaces based on the diurnal cycle, Earth Syst. Dynam., 8, 849–864, 2017.

Kleidon, A., Malhi, Y., and Cox, P. M.: Maximum entropy production in environmental and ecological systems, Phil. Trans. R. Soc. B, 365,
30   1297–1302, 2010.

Kleidon, A., Renner, M., and Porada, P.: Estimates of the climatological land surface energy and water balance derived from maximum convective power, Hydrol. Earth Syst. Sci., 18, 2201–2218, 2014.

Kleidon, A., Kravitz, B., and Renner, M.: The hydrologic sensitivity to global warming and solar geoengineering derived from thermodynamic constraints, Geophys. Res. Lett., pp. 138–144, 2015.

35 Liu, H., Zhang, Y., Liu, S., Jiang, H., Sheng, L., and Williams, Q. L.: Eddy covariance measurements of surface energy budget and evaporation in a cool season over southern open water in Mississippi, J. Geophys. Res., 114, D04 110, 2009.

Lorenz, R. D., Lunine, J. I., Withers, P. G., and McKay, C. P.: Titan, Mars and Earth: Entropy production by latitudinal heat transport, Geophys. Res. Lett., 28, 415–418, 2001.

Louis, J. F.: A parametric model of vertical eddy fluxes in the atmosphere, Boundary Layer Meteorology, 17, 187–202, 1979.

Martyushev, L. M. and Seleznev, V. D.: Maximum entropy production principle in physics, chemistry, and biology, Physics Reports, 426,
5   1–45, 2006.

Mueller, B. and Seneviratne, S. I.: Systematic land climate and evapotranspiration biases in CMIP5 simulations, Geophys. Res. Lett., 41, 128–134, 2014.

Newey, W. K. and West, K. D.: Automatic Lag Selection in Covariance Matrix Estimation, Review of Economic Studies, 61, 631–653, 1994.

Oke, T. R.: Boundary layer climates, Routledge, London and New York, second edition edn., 1987.

10   Ozawa, H. and Ohmura, A.: Thermodynamics of a global-mean state of the atmosphere – A state of maximum entropy increase, J. Clim., 10, 441–445, 1997.

Ozawa, H., Ohmura, A., Lorenz, R. D., and Pujol, T.: The second law of thermodynamics and the global climate system – A review of the Maximum Entropy Production principle, Rev. Geophys., 41, 1018, 2003.

Paltridge, G. W.: The steady-state format of global climate, Q. J. Roy. Meteorol. Soc., 104, 927–945, 1978.

15   Pauluis, O. and Held, I. M.: Entropy budget of an atmosphere in radiative convective equilibrium. Part I: Maximum work and frictional dissipation, J. Atmos. Sci., 59, 126–139, 2002a.

Pauluis, O. and Held, I. M.: Entropy budget of an atmosphere in radiative convective equilibrium. Part II: Latent heat transport and moist processes, J. Atmos. Sci., 59, 140–149, 2002b.

Raz-Yaseef, N., Billesbach, D. P., Fischer, M. L., Biraud, S. C., Gunter, S. A., Bradford, J. A., and Torn, M. S.: Vulnerability of crops and
20   native grasses to summer drying in the U.S. Southern Great Plains, Agriculture, Ecosystems and Environment, 213, 209–218, 2015.

Renno, N. O. and Ingersoll, A. P.: Natural convection as a heat engine: A theory for CAPE, J. Atmos. Sci., 53, 572–585, 1996.

Rocha, A. V. and Shaver, G. R.: Burn severity influences post-fire CO_2 exchange in arctic tundra, Ecological Applications, 21, 477–489, 2011.

Rotenberg, E. and Yakir, D.: Contribution of semi-arid forests to the climate system, Science, 327, 451–454, 2010.

25   Rotenberg, E. and Yakir, D.: Distinct patterns of changes in surface energy budget associated with forestation in the semiarid region, Glob. Ch. Biol., 17, 1536–1548, 2011.

Zeileis, A.: Econometric Computing with HC and HAC Covariance Matrix Estimators, Journal of Statistical Software, 11, 1–17, 2004.

Table 1. Variables and parameters used in this study.

Symbol	Variable	Units	Use or Assumption
D	Frictional dissipation	W m^{-2}	Assumed to be in steady state, with $D = G$
G	Convective power	W m^{-2}	Eq. (1), (3), (4)
J_{in}	Turbulent fluxes of sensible and latent heat	W m^{-2}	Eq. (1), (2), (5)
J_{opt}	Turbulent fluxes J_{in} optimized to yield max. power	W m^{-2}	Eq. (7)
J_{out}	Cooling rate of the heat engine	W m^{-2}	Eq. (1), (2)
k	Radiative parameterization constant	W m^{-2} K^{-1}	Used in linearization of $R_{l,net}$
$R_{l,out}$	Flux of terrestrial radiation to space	W m^{-2}	Assumed to be in steady state, with $R_{l,out} = R_{s,avg}$
R_s	Surface absorption of solar radiation	W m^{-2}	Forcing
$R_{s,avg}$	Surface absorption of solar radiation (average)	W m^{-2}	Eq. (6)
dU_a/dt	Change in atmospheric heat storage	W m^{-2}	Eq. (1), (2), (6)
T_a	Atmospheric temperature	K	Assumed to be the radiative temperature
T_e	Temperature of the heat engine	K	Assumed to be similar to the surface temperature
T_s	Surface temperature	K	–
dU_s/dt	Change in ground heat storage (or ground heat flux)	W m^{-2}	Prescribed from observations, Eq. (6)
dU_{tot}/dt	Change in total heat storage	W m^{-2}	Eq. (6)

Table 2. Site description of the six sites used for evaluating the estimations of the maximum power limit (with the letters referring to the graphs shown in Fig. 3). Also shown are the correlation statistics of the comparison to observations. Adjusted squared explained variance of the linear regression of J_{opt} to observed net radiation ($R_n = R_s - R_{l,net}$) minus ground heat flux $R_n - dU_s/dt$ is reported as r^2. Standard error of slope and intercept of the regression are derived by a prewhitening procedure to reduce the effect of serial correlation of the residuals (Newey and West, 1994; Zeileis, 2004).

Site	Description	r^2	Slope	Intercept	Reference
A	Tundra (Open Shrubland), USA	0.972	1.138	-54.80	Rocha and Shaver (2011)
	Anaktuvuk River (unburned site)		± 0.019	± 5.17	doi:10.17190/AMF/1246144
	68°56'N 150°16'W				
	Data used for June 2009, $n = 1392$				
B	Cropland, USA	0.993	1.106	-73.30	Fischer et al. (2007); Raz-Yaseef et al. (2015)
	ARM Southern Great Plains site		± 0.015	± 5.04	doi:10.17190/AMF/1246027
	36°36'N 97°29'W				
	Data used for June 2009, $n = 1060$				
C	Temperate Grassland, Germany	0.982	1.099	-36.38	Beyrich et al. (2006)
	DWD Falkenberg boundary layer site		± 0.012	± 3.56	
	52°10'N 14°7'E				
	Data used for June 2009, $n = 1440$				
D	Pine forest, Germany	0.982	1.023	-37.87	Beyrich et al. (2006)
	DWD Falkenberg boundary layer site		± 0.011	± 4.34	
	52°11'N 13°57'E				
	Data used for June 2009, $n = 1438$				
E	Pine forest, Israel	0.998	1.086	-53.87	Rotenberg and Yakir (2010, 2011)
	Yatir forest		± 0.006	± 2.22	
	31°20'N 35°3'E				
	Data used for June 2006, $n = 1440$				
F	Tropical rainforest, Brazil	0.999	0.995	-59.82	Goulden et al. (2004)
	Santarem km83 logged forest		± 0.003	± 1.23	doi:10.17190/AMF/1245995
	3°1'S 54°58'W				
	Data used for June 2002, $n = 1053$				